Miniaturized High Gain Flexible Spiral Antenna Tested in Human-Like Tissues

Miguel Fernandez-Munoz[iD], Rocio Sanchez-Montero[iD], Pablo Luis Lopez-Espi[iD], Juan A. Martinez-Rojas[iD], Efren Diez-Jimenez[iD]

***Abstract*— A miniaturized helical antenna is presented in this work. The antenna is flexible, it is 6100 µm long and it has a diameter of 352 µm. This antenna has such a small cross-section, that permits to be implanted in the human body with fine syringes and minimally invasive surgeries. The antenna can be used to receive power and/or send information in medical devices. The antenna is made of biocompatible materials: polytetrafluoroethylene (PFTE) and copper. The fundamental parameters of the antenna have been simulated and experimentally measured in animal human-like tissues, showing good agreement. The resonant frequency of the antenna is 4.7 GHz, with a reflection coefficient of -25.1 dB, and a gain of -4.7 dBi. As expected, the resonant frequency decreases inside biological tissues comparing to the free-space open-air measurement. Reducing the resonant frequency is an advantage because power signals can penetrate deeper into body tissues.**

***Index Terms*— Wireless Power Transfer (WPT), Helical Antenna, Spiral Antenna, Miniaturized Flexible Thin Antenna, Implantable Medical Device (IMD), High Gain Antenna.**

I. Introduction

THE wireless power transfer (WPT) [1] is a technology developed to power devices without the need of cables or batteries. WPT systems are composed of an external power source that emits signals and a receiver that captures the RF signal and transforms the energy. The receiving system is composed of at least two parts: an antenna to capture RF electromagnetic energy and the circuitry which transforms and condition the received signal to energize devices.

WPT systems have multiple uses in the medical area, as it can power implantable devices or surgical tools [2], [3]. These systems allow to do in-body measurements and send information to external receivers [4], [5], or to energize micro actuators [6]. These applications operate without the need for a physical connection between emitter and receiver. WPT systems also eliminate the need for batteries, which are required in a lot of medical implantable devices. The batteries have the drawback of their big size and the risk of the infections due to the non-biocompatible materials of batteries. With WPT systems, lifetime of the devices is not limited by the battery.

The resonant frequency of the antennas typically decreases inversely proportional to the antenna size [7], [8]. This effect imposes a main obstacle to obtain miniaturized antennas working at low frequencies [9], [10]. The electromagnetic energy absorption of human body is highly dependent on electromagnetic wave frequency. The percentage of absorption is negligible for frequencies lower than 100 MHz. The energy absorbed by the human body increases progressively for frequencies from 100 MHz up to 5 THz. Above 5 THz, the absorption decreases again until 10^{17} Hz, where X-rays penetrate completely [11]. This behavior is similar to the electromagnetic absorption behavior of water.

For medical applications, increasing the emitted power is not sometimes a solution to overcome body absorption because there are radiation limits, defined in ICNIRP guideline [12] and IEEE Standards Coordinating Committee [13], that can not be overpassed. For example, the peak limit defined by the ICNIRP Guidelines 2020, considering occupational, local exposure, and a frequency of 4.7 GHz, it is 200 µW/mm^2. Besides, it is important to limit the emitted power to maintain a safe local temperature, not to exceed the limit of 43ºC that could cause injuries. There is a correlation between the Specific Absorption Rate (SAR) and the temperature increase in areas close to the implantable receivers [14]. The decisive factor which determines the temperature increase is blood flow around the position where peak SAR appears.

In this paper, an ultrathin high gain miniaturized flexible helical antenna is proposed. The antenna is made of biocompatible materials: copper and polytetrafluoroethylene (PFTE). The antenna has been designed using a combination of model based system engineering and trade-off analysis [15]. The helical antenna morphology was chosen because it can achieve lower resonant frequencies and higher gain values than other morphologies, with reduced cross section diameters. In addition, its elongated shape contributes to flexibility. Comparing with the most similar one found in the literature

Manuscript received **********; revised **********; accepted *******. Date of publication **********; date of current version **********. This work was supported by the European Union's Horizon 2020 research and innovation programme under grant agreement No 857654–UWIPOM2, and by Universidad de Alcalá within the framework of the Predoctoral Contracts for the Training of Research Staff (2021). The review of this article was arranged by guest editors of the Special Issue for NanoCoCoA 2021. *(Corresponding author: Miguel Fernández Muñoz)*

Miguel Fernández Muñoz and Efrén Díez Jiménez are with the Universidad de Alcalá (Spain), Signal Theory and Communications Department, Mechanical Engineering Area. (e-mail: miguel.fm@uah.es; efren.diez@uah.es)

Rocío Sánchez Montero, Pablo Luis López Espí and Juan Antonio Martínez Rojas are with the Universidad de Alcalá (Spain), Signal Theory and Communications Department. (e-mail: rocio.sanchez@uah.es; pablo.lopez@uah.es; juanan.martinez@uah.es)

Digital Object Identifier **********

[16], the proposed antenna has a dielectric core that reduces the resonant frequency, while giving it structural stability. The design has been optimized in terms of resonant frequency and size, to work below the 5GHz practical limit of body absorption. The simulated and measured fundamental parameters are shown. Simulations and measurements of the antenna in open-air and between human-like tissues are also presented and compared. Moreover, the flexible behavior of the antenna is demonstrated. This antenna can power micro-robotic actuators and terminal catheter tools and/or send information with the appropriate microelectronics.

II. State of the Art

The state of the art is focused on miniaturized antennas with lowest resonant frequencies. An antenna similar to the one proposed in this article is presented in reference [16]. This antenna has a ~0.2 mm diameter and a length of 5.5 mm. Its resonant frequency is 5.8 GHz (ISM-Band). The drawback of this antenna is its low gain, that is -46 dBi. A polarized helical antenna for ISM-Band (2.4–2.48 GHz) with a radius of 5.5 mm and a thickness of 3.81 mm is presented in reference [17]. In reference [18], a helical antenna that works at the L1/L2 GPS band (1575.42 and 1227.60 MHz) is described. The antenna has a diameter of 12 mm and a height of 24.7 mm. A quadrifilar helical antenna that resonates at L1/L5 GPS bands (1575.42 and 1176 MHz) is detailed in [19]. It has a diameter of 36 mm and an axial length of 72.48 mm. The antennas presented in [17]–[19] have a resonant frequency suitable for working inside the human body, but they are not flexible and their dimensions are much larger than the one presented in this article. Some flexible helical antennas have also been found, of longer length. Authors of [20] describe a helical dipole antenna for ablation. It works at 1.9 GHz, and it has a diameter of 1.64 mm and a length of 23 mm. In [21], the proposed antenna operates at 865 MHz, but it has a 0.8 mm diameter and a 34.4 mm length.

From another point of view, there are some studies at nanoscale, discussing antennas that work at higher frequencies [22], but they usually resonate near the Terahertz range. For example, a carbon nanotube antenna is presented in [23], and an investigation of multiwall carbon nanotubes is explained in [24]. Some nanofilm microstrip antennas that resonate around 12 GHz are experimentally characterized in [25]. The resonant frequencies of all these Terahertz range antennas are far from 10^{17} Hz, where they would be very useful for internal medical uses.

III. Antenna Design

The helical antenna cross section has been adjusted to permit insertion of the antenna using fine syringes or catheters. In addition, the resonant frequency has been reduced to minimize absorption in the human body. The structure of the antenna is based on a double spiral (helical antenna), with two arms of 30 turns of copper wire, having a pitch of 100 µm. The copper is wound around a thin hollow flexible cylinder (core). The core is a 6100 µm long PFTE cylinder from the GoodFellow company, Huntingdon, England. The core has an external diameter of 300 µm and an internal diameter of 100 µm. It keeps the antenna stiff enough while making it flexible.

The wire is the HSP15 Solabond from the Elektrisola company, Reichshof-Eckenhagen, Germany. This wire has a nominal diameter of 20 µm. It also has two layers of self-adhesive polyurethane and polyamide. This wire provides high bond strength, it is non-hygroscopic, and it is also biocompatible. This allows to have a high number of turns in a short length and does not complicate the manufacturing excessively.

The antenna feed is located in the middle, and the antenna presents a 16 Ω balanced port impedance. Thus, a matching circuit would be required to connect the antennas to a standard 50 Ω port. Figure 1 shows the antenna design. The dimensions are given in Table 1.

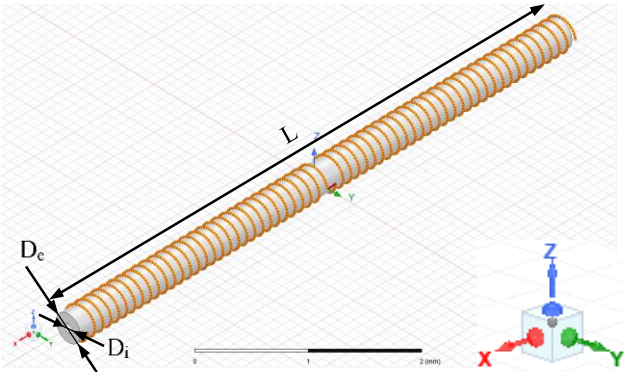

Figure 1: Antenna design.

TABLE 1
DIMENSIONS OF THE ANTENNA

Parameter	Dimension (µm)
Length (L)	6100
External diameter (D_e)	300
Internal Diameter (D_i)	100
Pitch	100
Wire diameter	20
Wire + coating diameter	26

IV. Antenna Electromagnetic Simulations

The antenna from Figure 1 has been simulated using the electromagnetic tool HFSS from Ansys Electronics [26]. Simulations were performed from 0 to 6.5 GHz, with a step of 0.1 GHz. The simulated resonant frequency of the antenna is 4.7 GHz with a reflection coefficient (S11) of -25.1 dB, and the maximum gain was -4.7 dBi. Then, the characteristic length of the antenna can be expressed as 0.039λ. The reflection coefficient as a function of frequency is shown in Figure 2.

The antenna cannot be connected to standard ports to measure its fundamental parameters because of the geometry and the size of the antenna, and the brittleness of the wire. Then, the ends of the wire were soldered to a printed circuit board (PCB) with copper pads, where miniature RF probes can lean on. This auxiliary assembly including the antenna, the PCB with copper pads, tin solders, and a layer of glue was also created in Ansys HFSS. The auxiliary model is shown in Figure

3, and the reflection coefficient is also shown in Figure 2. The simulated resonant frequency was 3.2 GHz, the reflection coefficient -19.6 dB, and the maximum gain -10.87 dBi.

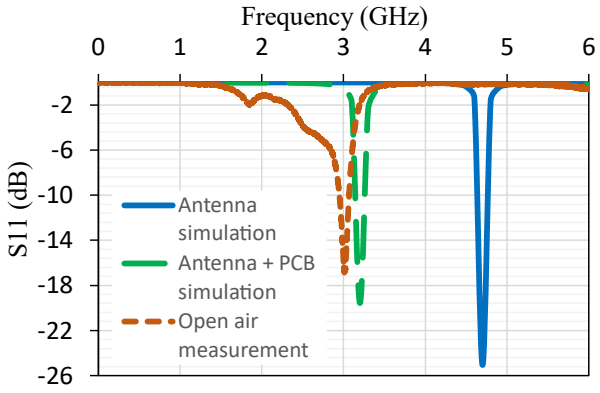

Figure 2: Reflection coefficient of the antenna (simulated) and the antenna + PCB (simulated and measured).

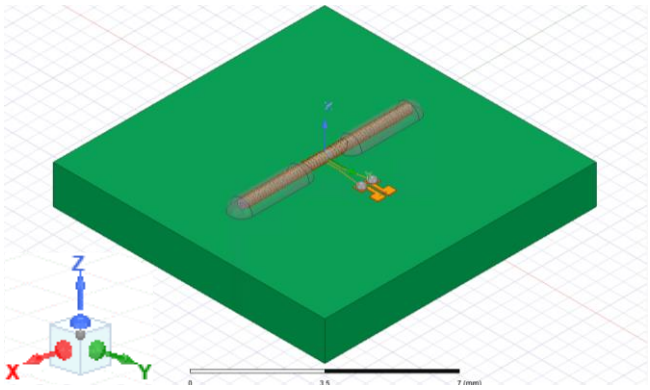

Figure 3: Antenna + PCB HFSS model (auxiliary assembly).

V. Measurement of the Fundamental Parameters of the Antenna

A. Resonant frequency and reflection coefficient measurements

The antenna was manufactured following the same winding technique as the microcoils shown in reference [27]. The antenna prototype is shown in Figure 4 a). The antenna was glued with high-strength fast-adhering cyanoacrylate-based glue to the PCB. Then, the wire ends were soldered to the copper pads, as in the auxiliary simulation model. The antenna with PCB auxiliary assembly is shown in Figure 4 b).

The resonant frequency and the reflection coefficient of the antenna were measured using a Keysight ENA E5063A Vector Network Analyzer, a MPI TITAN RF probe T26A-SG0200, and digital microscopes for the positioning of the RF probe. The measured reflection coefficient is shown in Figure 2. A resonant frequency of 3 GHz with a reflection coefficient of -17 dB was measured. The measured resonant frequency is close to the simulated one for the auxiliary assembly, and the reflection coefficient is 13.3% higher. This difference comes from the impedance of the probe, which is 50 Ω, while the impedance of the antenna in the PCB is 16 Ω. A matching circuit would be necessary to adapt the antenna impedance to that of the circuit to which it is connected. As there is good agreement between simulation and measurement of the antenna + PCB, it can be inferred that the antenna without PCB would behave as the simulation results show in Figure 2, i.e., with a resonant frequency of 4.7 GHz.

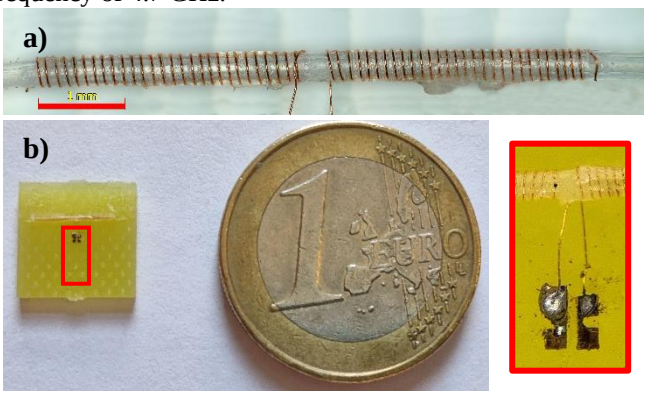

Figure 4: a) Manufactured antenna. b) Antenna with PCB (auxiliary assembly) compared with one-euro coin.

B. Gain and radiation pattern measurements

The gain and the radiation pattern of the microantenna were experimentally determined. A broadband horn antenna TEMH 6000 has been used as emitter antenna. TEHM 6000 is a calibrated antenna with a nominal frequency range of 380MHz to 6 GHz, and an isotropic gain of 2 to 10 dBi. The emitter antenna and the helical antenna under test were placed aligned one opposite the other and at a distance greater than 5 wavelengths, to perform the test in the far field region. Since the resonant frequency is 3GHz, the wavelength is obtained with the following expression:

$$\lambda = \frac{c}{f} = \frac{3 \cdot 10^8}{3 \cdot 10^9} = 0.1\ m \quad (1)$$

The separation was set at 0.5 m. The emitter antenna was connected to an Agilent 8665B Synthesized Signal Generator, and the antenna under test to an Agilent N9010A EXA Signal Analyzer using a MPI TITAN RF probe model T26A-GS0250. A rotation stage was used to allow the receiving antenna to be rotated while its radiation pattern is determined.

The received power was measured, and the gain of the antenna at its resonant frequency was determined using the Friis Equation, as follows:

$$(G_{AR})_{db} = (P_R)_{db} - (P_T)_{db} - (G_{AT})_{db} - 20 \cdot \log(\lambda) + 20 \cdot \log(D \cdot 4 \cdot \pi) \quad (2)$$

The measured gain was -4.69 dBi. This gain is more than 35dB better than the gain of the antenna shown in reference [16]. The fact that the antenna has a much larger number of turns than the one shown in reference [16], increases the electrical length of the antenna, thus reducing the frequency. The use of a dielectric inner core also helps to increase the gain and reduce the resonant frequency. The receiver antenna was then rotated at a constant transmitted power to determine the radiation pattern. The normalized simulated radiation pattern is shown in Figure 5 (red), and the measured one in Figure 5 (blue) for comparison.

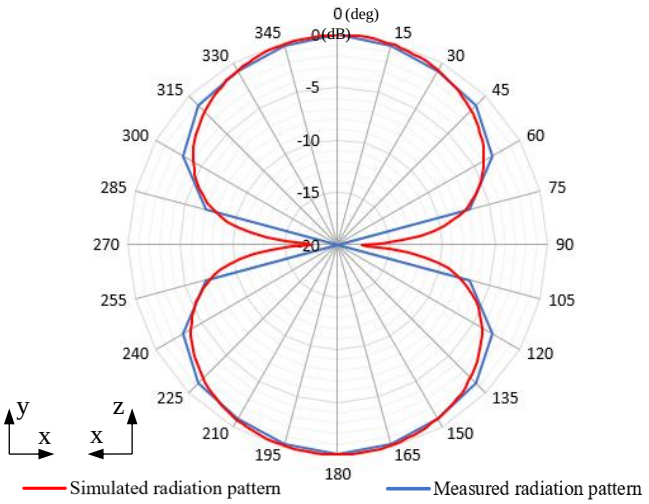

Figure 5: Simulated and measured radiation patterns of planes XY and XZ (symmetrical).

Figure 5 shows the total gain radiation pattern of the planes XY and XZ (see coordinate system of Figure 1 or 3), that are the ones that include the axis of the antenna. This radiation pattern has a null point at 90º degrees, which is the direction of the axis of the antenna. As the antenna is an axisymmetric body, the radiation pattern in any other plane that contains the axis of the antenna will be the same. In the plane YZ, the one perpendicular to the axis, the antenna shows an omnidirectional pattern with the maximum gain.

VI. Flexibility Study

The flexibility of the antenna has been tested. This antenna requires a high capacity for flexible deformation to facilitate its implantation by minimally invasive techniques.

One antenna prototype was manually folded and stretched several times by using two small tweezers, reaching angles of less than 40º. Some photos of the bending procedure are shown in Figure 6. The antenna did not break during the test, and it works correctly after the flexibility test. An angle of 40° is considered sufficiently acute to implant the antenna through the intricate vascular pathways. The curvature radius of the proposed antenna is in the order of 1-2 mm, much smaller than that of other flexible antennas, with radius of 10 mm [20]. And, as it is elastically flexible, it recovers its original straight shape.

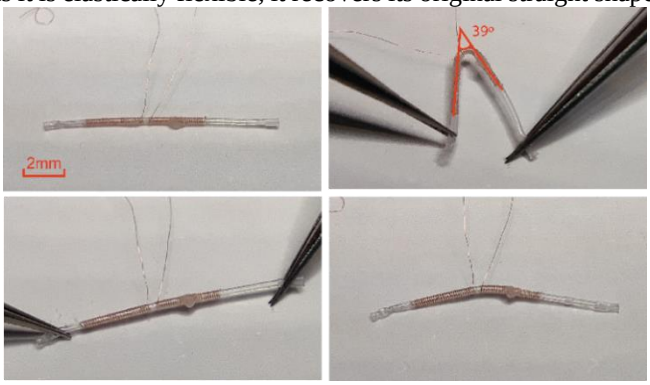

Figure 6: Flexibility study of the antenna.

VII. Simulations with the Antenna Between Human-Like Tissues

The final target operational environment for the antenna is inside human body. Thus, simulations and measurements were performed in human-like conditions to understand the antenna behavior in this environment. The HFSS model with the antenna + PCB was also simulated, wrapping the assembly between muscle and fat solid blocks. The dielectric properties for the muscle and fat tissues were defined at the resonant frequency of 3.22 GHz. Muscle was defined with a relative permittivity 51.8 and a bulk conductivity of 2.32 Siemens/m. Fat was defined with a relative permittivity of 10.6 and a conductivity 0.377 of Siemens/m [28]. Several models with the antenna on and between the tissues were simulated, Figure 7.

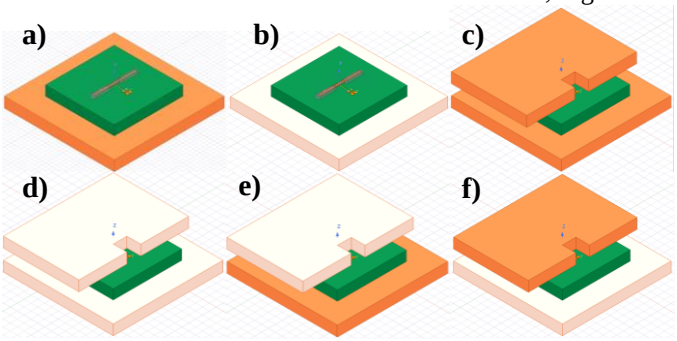

Figure 7: Human-like tissue simulation models: a) on muscle, b) on fat, c) between muscle, d) between fat, e) between muscle and fat, f) between fat and muscle.

The simulated reflection coefficient for each case, compared to the measurements, is shown in Figure 9 and 10. The resonant frequency decreases if the antenna is surrounded by the tissues, being lower when surrounded by muscle than by fat.

VIII. Measurements with the Antenna in Animal Human-Like Tissues

The simulated scenarios were replicated in experiments using pork muscle and fat. The antenna reflection coefficient was measured with fresh tissues pieces above, below and surrounding the antenna, as shown in Figure 8.

Figure 8: Antenna between human-like tissue measurements. On the left, antenna surrounded by pork muscle tissues. On the right, antenna surrounded by pork fat tissues.

The measured reflection coefficients of the antenna surrounded by human-like tissues compared with the simulations are shown in Figures 9 and 10.

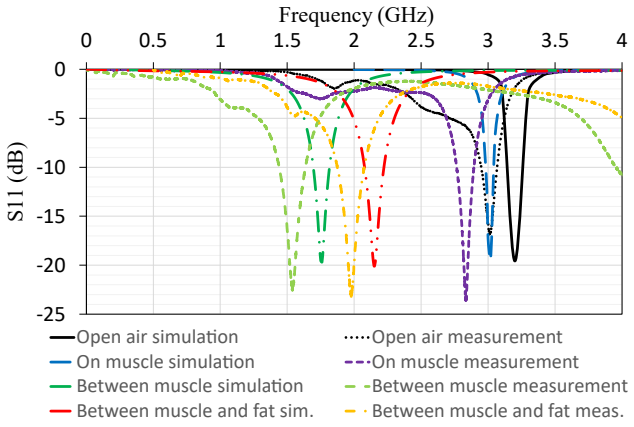

Figure 9: Reflection coefficient measurements and simulations of the antenna in open air and surrounded by muscle tissues.

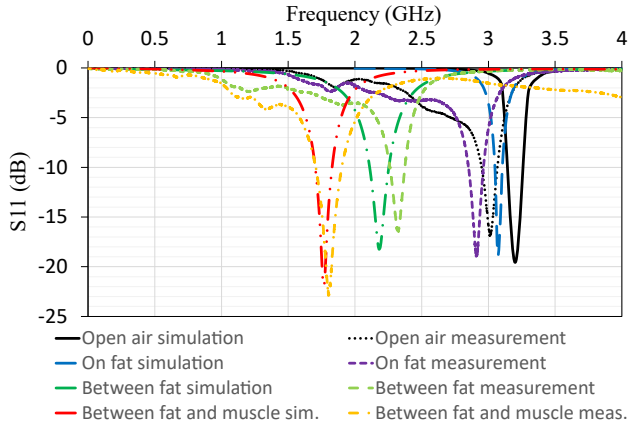

Figure 10: Reflection coefficient measurements and simulations of the antenna in open air and surrounded by fat tissues.

It was found that the resonant frequency does not change more than 7.5% of the resonant frequency in open air measurement for the measurements over muscle and on fat. In contrast, in the rest of the cases, in which there is a tissue above, the frequency decreases significantly. Actually, when the antenna is placed between muscle tissues, the resonant frequency is halved. This is actually an advantage, as a lower resonant frequency increases transmission efficiency in the human body. Nevertheless, if the antenna were implanted, the surrounding environment would be constant, and the resonant frequency of the antenna would also be constant. With adequate isolation, the resonant frequency would not change.

The energy transmission efficiency at the resonant frequency of the antenna, and other frequencies of interest, has been studied, depending on the depth of penetration and the type of tissue. Values for penetration depth given in reference [29] have been used. Penetration depth is determined as the distance at which the power density is reduced by e^{-2} (13.5%). High content water (HCW) tissues are muscles and skin, and low water content (LWC) tissues are fat and bones. Thus, the following and relations can be extracted:

$$HCW\ tissues: \quad f(x) = 2.1568x^{-0.616} \quad (2)$$

$$LCW\ tissues: \quad f(x) = 16.391x^{-0.598} \quad (3)$$

From (2) and (3), the transmission efficiency through the tissues has been determined, and it is shown in Figures 11 and 12.

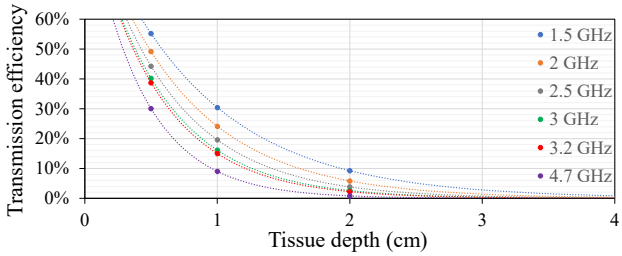

Figure 11: Transmission efficiency of a signal through HCW tissues.

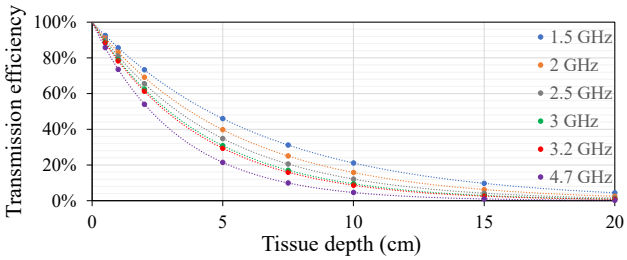

Figure 12: Transmission efficiency of a signal through LCW tissues.

The transmission efficiency is better through LCW than HCW. In all cases, the efficiency is higher through thin tissues and at lower frequencies. It is demonstrated that the observed effect of lowering the resonant frequency while the antenna is surrounded by tissues is beneficial for the transmission.

IX. Conclusion

We have presented an ultrathin flexible high gain helical antenna prototype with a millimeter size suitable for WPT systems. The dimensions of the prototype are: 352 µm outer diameter, 100 µm inner diameter and 6100 µm length. This allows the antenna to be implanted inside the body with minimally invasive surgeries. Additionally, it can be attached to thin catheters to receive and supply power to the actuators at the catheter end. The antenna has been manufactured using biocompatible materials: PTFE for the inner cylinder and copper for the helix. The flexibility of the antenna has been demonstrated.

The simulations show that the antenna resonates at 4.7 GHz with -4.7 dBi of gain. The resonant frequency can be adjusted by increasing or decreasing the number of turns, making the antenna very versatile. The simulation model was validated with measurements. The measured resonant frequency, with the antenna soldered to a PCB is 3 GHz, in good agreement to the simulated resonant frequency of 3.2 GHz. The measured gain is -4.7 dBi. The validation of this simulation model allows to infer that the antenna without the PCB will behave as expected from the simulations.

Finally, simulations and measurements were performed with the antenna surrounded by pork muscle and fat. The resonant

frequency of the antenna surrounded by tissues decreases with respect to the resonant frequency in open-air measurements, being lower inside muscles than inside fat. Reducing the operational frequency is highly beneficial to increase efficiency in the transmission link for in-body applications.

ACKNOWLEDGMENT

This research has been supported by the European Union's Horizon 2020 research and innovation programme under grant agreement No 857654–UWIPOM2. This work has also been funded by Universidad de Alcalá within the framework of the Predoctoral Contracts for the Training of Research Staff (2021).

The authors want to recognize the work of Alba Martinez-Perez during preparation of the figures.

REFERENCES

[1] Z. Zhang, H. Pang, A. Georgiadis, and C. Cecati, "Wireless Power Transfer - An Overview," *IEEE Trans. Ind. Electron.*, vol. 66, no. 2, pp. 1044–1058, Feb. 2019.

[2] M. Haerinia and R. Shadid, "Wireless Power Transfer Approaches for Medical Implants: A Review," *Signals*, vol. 1, no. 2, pp. 209–229, 2020.

[3] A. Kiourti and K. S. Nikita, "A review of in-body biotelemetry devices: Implantables, ingestibles, and injectables," *IEEE Trans. Biomed. Eng.*, vol. 64, no. 7, pp. 1422–1430, 2017.

[4] K. Kim, S. Yun, S. Lee, S. Nam, Y. J. Yoon, and C. Cheon, "A design of a high-speed and high-efficiency capsule endoscopy system," *IEEE Trans. Biomed. Eng.*, vol. 59, no. 4, pp. 1005–1011, 2012.

[5] S. H. Lee *et al.*, "A wideband spiral antenna for ingestible capsule endoscope systems: Experimental results in a human phantom and a pig," *IEEE Trans. Biomed. Eng.*, vol. 58, no. 6, pp. 1734–1741, 2011.

[6] G. Villalba-Alumbreros, C. Moron-Alguacil, M. Fernandez-Munoz, I. Valiente-Blanco, and E. Diez-Jimenez, "Scale Effects on Performance of BLDC Micromotors for Internal Biomedical Applications: A Finite Element Analysis," *J. Med. Device.*, vol. 16, no. 3, Sep. 2022.

[7] L. J. Chu, "Physical Limitations of Omni-Directional Antennas," *J. Appl. Phys.*, vol. 19, no. 12, pp. 1163–1175, Dec. 1948.

[8] R. F. Harrington, "Effect of antenna size on gain, bandwidth, and efficiency," *J. Res. Natl. Bur. Stand. Sect. D Radio Propag.*, vol. 64D, no. 1, p. 1, Jan. 1960.

[9] A. H. Safavi-Naeini and O. Ramahi, "Miniaturizing the axial mode helical antenna," *HUT-ICCE 2008 - 2nd Int. Conf. Commun. Electron.*, pp. 374–379, 2008.

[10] A. Ibrahim and M. Kiani, "A Figure-of-Merit for Design and Optimization of Inductive Power Transmission Links for Millimeter-Sized Biomedical Implants," *IEEE Trans. Biomed. Circuits Syst.*, vol. 10, no. 6, pp. 1100–1111, 2016.

[11] P. Lannoye, *La Pollution électromagnétique et la santé : vers une maîtrise des risques*. Frison-Roche, 1994.

[12] G. Ziegelberger *et al., Guidelines for limiting exposure to electromagnetic fields (100 kHz to 300 GHz)*, vol. 118, no. 5. 2020.

[13] W. H. Bailey *et al., Synopsis of IEEE Std C95.1™-2019 "IEEE Standard for Safety Levels with Respect to Human Exposure to Electric, Magnetic, and Electromagnetic Fields, 0 Hz to 300 GHz,"* vol. 7. 2019.

[14] A. Hirata, O. Fujiwara, and T. Shiozawa, "Correlation between peak spatial-average SAR and temperature increase due to antennas attached to human trunk," *IEEE Trans. Biomed. Eng.*, vol. 53, no. 8, pp. 1658–1664, 2006.

[15] J. A. Martínez Rojas, J. L. Fernández, R. S. Montero, P. L. L. Espí, and E. Diez-Jimenez, "Model-based systems engineering applied to trade-off analysis of wireless power transfer technologies for implanted biomedical microdevices," *Sensors*, vol. 21, no. 9, 2021.

[16] D. D. Karnaushenko, D. Karnaushenko, D. Makarov, and O. G. Schmidt, "Compact helical antenna for smart implant applications," *NPG Asia Mater.*, vol. 7, no. 6, p. 188, Jun. 2015.

[17] C. Liu, Y. X. Guo, and S. Xiao, "Circularly polarized helical antenna for ISM-band ingestible capsule endoscope systems," *IEEE Trans. Antennas Propag.*, vol. 62, no. 12, pp. 6027–6039, 2014.

[18] Y. Han *et al.*, "Dual-Band Spiral Printed Quadrifilar Helical Antenna Miniaturized by Surface and Inner Dielectric Loading," *IEEE Access*, vol. 7, pp. 30244–30251, 2019.

[19] J. Rabemanantsoa and A. Sharaiha, "Size reduced multi-band printed quadrifilar helical antenna," *IEEE Trans. Antennas Propag.*, vol. 59, no. 9, pp. 3138–3143, 2011.

[20] Y. Mohtashami, N. Behdad, and S. C. Hagness, "Ex Vivo Performance of a Flexible Microwave Ablation Antenna," *IEEE Trans. Biomed. Eng.*, vol. 68, no. 5, pp. 1680–1689, 2021.

[21] L. Zou, C. McLeod, and M. R. Bahmanyar, "Wireless Interrogation of Implantable SAW Sensors," *IEEE Trans. Biomed. Eng.*, vol. 67, no. 5, pp. 1409–1417, 2020.

[22] P. J. Burke, S. Li, and Z. Yu, "Quantitative theory of nanowire and nanotube antenna performance," *IEEE Trans. Nanotechnol.*, vol. 5, no. 4, pp. 314–334, 2006.

[23] S. F. Mahmoud and A. R. AlAjmi, "Characteristics of a new carbon nanotube antenna structure with enhanced radiation in the sub-terahertz range," *IEEE Trans. Nanotechnol.*, vol. 11, no. 3, pp. 640–646, 2012.

[24] A. R. Alajmi and S. F. Mahmoud, "Investigation of multiwall carbon nanotubes as antennas in the subterahertz range," *IEEE Trans. Nanotechnol.*, vol. 13, no. 2, pp. 268–273, 2014.

[25] F. Urbani, D. W. Stollberg, and A. Verma, "Experimental characterization of nanofilm microstrip antennas," *IEEE Trans. Nanotechnol.*, vol. 11, no. 2, pp. 406–411, 2012.

[26] "Ansys HFSS | 3D High Frequency Simulation Software." [Online]. Available: https://www.ansys.com/products/electronics/ansys-hfss. [Accessed: 15-Mar-2022].

[27] E. Diez-Jimenez *et al.*, "Multilayered Microcoils for Microactuators and Characterization of Their Operational Limits in Body-Like Environments," *IEEE/ASME Trans. Mechatronics*, pp. 1–6, 2022.

[28] "Dielectric Properties » IT'IS Foundation." [Online]. Available: https://itis.swiss/virtual-population/tissue-properties/database/dielectric-properties/. [Accessed: 05-Sep-2022].

[29] M. de T. y A. S. de España, "Nota Técnica de Prevención 234 Exposición a Radiofrecuencias y Microondas (I). Evaluación," 1984.